Human Molecular Genetics, 2018, Vol. 27, No. 11 1892–1904

doi: 10.1093/hmg/ddy096
Advance Access Publication Date: 14 March 2018
Original Article

ORIGINAL ARTICLE

Defective kinesin binding of TUBB2A causes progressive spastic ataxia syndrome resembling sacsinopathy

Antonella Sferra[1,2], Fabiana Fattori[1,2], Teresa Rizza[1,2], Elsabetta Flex[3], Emanuele Bellacchio[2], Alessandro Bruselles[3], Stefania Petrini[4], Serena Cecchetti[5], Massimo Teson[6], Fabrizia Restaldi[7], Andrea Ciolfi[2], Filippo M. Santorelli[8], Ginevra Zanni[1,2], Sabina Barresi[2], Claudia Castiglioni[9], Marco Tartaglia[2] and Enrico Bertini[1,2,*]

[1]Unit of Neuromuscular and Neurodegenerative Disorders, Department Neurosciences, [2]Genetics and Rare Diseases Research Division, Ospedale Pediatrico Bambino Gesù, 00146 Rome, Italy, [3]Department of Oncology and Molecular Medicine, Istituto Superiore di Sanità, 00161 Rome, Italy, [4]Confocal Microscopy Core Facility, Research Laboratories, Ospedale Pediatrico Bambino Gesù, 00146 Rome, Italy, [5]Confocal Microscopy Unit, Core Facilities, Istituto Superiore di Sanità, 00161 Rome, Italy, [6]Laboratory of Molecular and Cell Biology, Istituto Dermopatico Dell'Immacolata IDI-IRCCS, 00167 Rome, Italy, [7]Unit of Medical Genetics, Department of Laboratories, Ospedale Pediatrico Bambino Gesù, 00146 Rome, Italy, [8]IRCCS Stella Maris, Molecular Medicine and Neuromuscular Disorders, 56128 Pisa, Italy and [9]Neurology Unit, Department of Pediatrics, Clínica Las Condes, 7550000 Santiago, Chile

*To whom correspondence should be addressed at: Unit of Neuromuscular and Neurodegenerative Disorders, Laboratory of Molecular Medicine, Ospedale Pediatrico Bambino Gesù IRCCS, V.le S. Paolo, 15, Polo di Ricerca S. Paolo, 00146 Rome, Italy. Tel: +390668592104; Fax: +306868592024; Email: ebertini@gmail.com

Abstract

Microtubules participate in fundamental cellular processes, including chromosomal segregation and cell division, migration and intracellular trafficking. Their proper function is required for correct central nervous system development and operative preservation, and mutations in genes coding tubulins, the constituting units of microtubules, underlie a family of neurodevelopmental and neurodegenerative diseases, collectively known as 'tubulinopathies', characterized by a wide range of neuronal defects resulting from defective proliferation, migration and function. Here, we causally link a previously unreported missense mutation in *TUBB2A* (c.1249G>A, p.D417N), encoding one of the neuron-specific β-tubulin isotype II, to a disorder characterized by progressive spastic paraplegia, peripheral sensory-motor polyneuropathy and ataxia. Asp^{417} is a highly conserved solvent-exposed residue at the site mediating binding of kinesin superfamily motors. Impaired binding to KIF1A, a neuron-specific kinesin required for transport of synaptic vesicle precursors of the disease-associated TUBB2A mutant, was predicted by structural analyses and confirmed experimentally *in vitro*. We show that overexpression of $TUBB2A^{D417N}$ disrupts the mitotic spindle bipolarity and morphology and affects the M phase entry and length. Differently

Received: December 29, 2017. **Revised:** March 12, 2018. **Accepted:** March 12, 2018

from the TUBB2A^{N247K} and TUBB2A^{A248V}, two mutants previously identified to affect neurodevelopment, TUBB2A^{D417N} retains the ability to assemble into microtubules. Consistent with the differential clinical and structural impact, TUBB2A^{A248V} does not drastically affect TUBB2A binding to KIF1A, nor mitotic spindle bipolarity. Overall, our data demonstrate a pathogenic role of the p.D417N substitution that is different from previously reported *TUBB2A* mutations and expand the phenotypic spectrum associated with mutations in this gene.

Introduction

Alpha and β-tubulins are the major components of microtubules, in which they are continuously incorporated and released, making these structures highly dynamic (1). Microtubules are implicated in a host of cellular functions (2) and are major cytoskeletal components of neurons, where their function is required for proper neuronal cell division, polarity, migration and intracellular trafficking (3). Consistently, nervous system development, and neuronal survival and function are highly dependent on proper microtubule function, and mutations in an increasing number of genes encoding for tubulin subunits (*TUBA1A*, *TUBA8*, *TUBB2B*, *TUBB3*, *TUBB2A* and *TUBB5*) have been associated with a wide spectrum of neurodevelopmental disorders, collectively known as 'tubulinopathies', mostly characterized by non-progressive complex cortical and brain malformations. The identification of heterozygous mutations in *TUBA4A* as the molecular cause of a progressive form of amyotrophic lateral sclerosis (4) supports the view that mutations in these genes may also underlie a greater proportion of neurodegenerative conditions than currently appreciated.

In mammals, there are at least seven β-tubulin isotypes, which are encoded by multiple genes with differential tissue expression (5,6). Among these, class I (TUBB1), class II (TUBB2) and class III (TUBB3) isoforms are strongly expressed in neurons (7–9). TUBB2A represents ∼30% of all β-tubulins in human brain (10), and mutations in this gene have recently been reported to cause a developmental disorder characterized by structural brain abnormalities, including cortical dysplasia, simplified gyral patterning, anterior temporal pachygyria and perisylvian polymicrogyria (11–13). So far, two disease-causing missense changes (c.741C>G, p.N247K; c.743C>T, p.A248V) have been reported (11), which have been shown to impair proper formation of the α/β-tubulin heterodimer, resulting in a decreased or impaired incorporation of β-tubulin into microtubule polymers.

Here, we report on the identification of a novel variant in *TUBB2A* identified by 'whole' exome sequencing (WES) in a subject with a condition characterized by progressive spastic ataxia and a sensory motor peripheral neuropathy resembling a sacsinopathy. We demonstrate that, differently from the previously identified *TUBB2A* mutations affecting neurodevelopment, the present disease-causing mutation impairs the affinity of microtubules to neuron-specific kinesin KIF1A and does not affect dramatically β-tubulin incorporation in microtubules. Notably, such perturbed function specifically affects the spindle assembly during mitosis. Our data associates this novel mutation in *TUBB2A* with a phenotype of progressive neurodegeneration and expands the phenotypic spectrum of β-tubulin 2A beyond structural brain defects and brain malformations or infantile-onset epilepsy.

Results

Clinical assessment

The patient, a 23-year-old young male was born to non-consanguineous parents of Italian ancestry. The clinical history was characterized by delayed motor milestones. He was able to sit around the age of 1 year and started to walk on tip toes at the age of 2 years. At age 4 years, he exhibited spastic paraplegia and an ataxic syndrome that slowly worsened with time with progressive gait difficulties, and onset of pyramidal signs limited to the upper limbs. Extensive metabolic investigations were performed but yielded negative results. Brain magnetic resonance imaging (MRI) at the age of 8 years showed periventricular T2 hyperintense areas. Multimodal evoked potentials documented normal somatosensory evoked responses, while visual evoked potentials were mildly delayed with a normal electroretinogram. Nerve conduction velocity studies documented that the sensory conduction velocity of the sural nerve was not evocable, while motor nerve conduction velocity of the right and left peroneal nerve was reduced to 22 m/s with low compund motor action potential (CMAP) amplitudes (left: 2.5 mVs and right 0.8 mVs), and that of the right ulnar nerve was delayed to 36 m/s with low normal CMAP amplitude (7.4 mVs). At follow up, reduced visual acuity with strabismus appeared together with progressive spasticity, ataxia and distal amyotrophy of hands and feet with bilateral foot drop (Fig. 1D and E). Neurological examination at the age of 17 documented loss of autonomous walking. Cognitive levels were somewhat sluggish and delayed. The Raven test was under 5%. He showed distal amyotrophy of hands and feet, strabismus and pendular nystagmus in all directions of gaze. Electromyography and conduction velocity examination suggested a motor axonal neuropathy for both the upper and lower limbs. Spasticity was severe in lower limbs showing bilateral foot clonus. Ophthalmological examination documented a bilateral temporal optic atrophy but there were aspects of macular dystrophy bilaterally in the absence of any sign of pigmental retinopathy. Optical coherence tomography (OCT) showed normal parameters (Fig. 1G). Control MRI performed at the age of 18 years showed atrophy of the superior cerebellar vermis, T2-hypointense stripes and thinning of the corpus callosum. The cognitive Wechsler-IV for adults detected a total score of 69, which was consistent with a mild mental defect. The MRI had features of cerebellar atrophy and hypointense stripes in the pons suggesting a sacsinopathy (Fig. 1A–C). Extensive molecular genetic analysis ruled out dominant spinocerebellar ataxias, hereditary spastic paraplegia syndromes and other neurodegenerative disorders by targeted resequencing using a comprehensive custom disease gene panel, including sacsin (SACS).

Molecular analysis

To identify the molecular event underlying the trait, exome sequencing was performed in the proband and unaffected parents and siblings. WES data output is summarized in Supplementary Material, Table S1. Among 87 392 called variants, data annotation predicted 11 938 high-quality variants having functional impact (i.e. non-synonymous and splice site changes). Among the latter, 323 were private or rare changes and were retained for further analyses. Variants predicted to be deleterious by

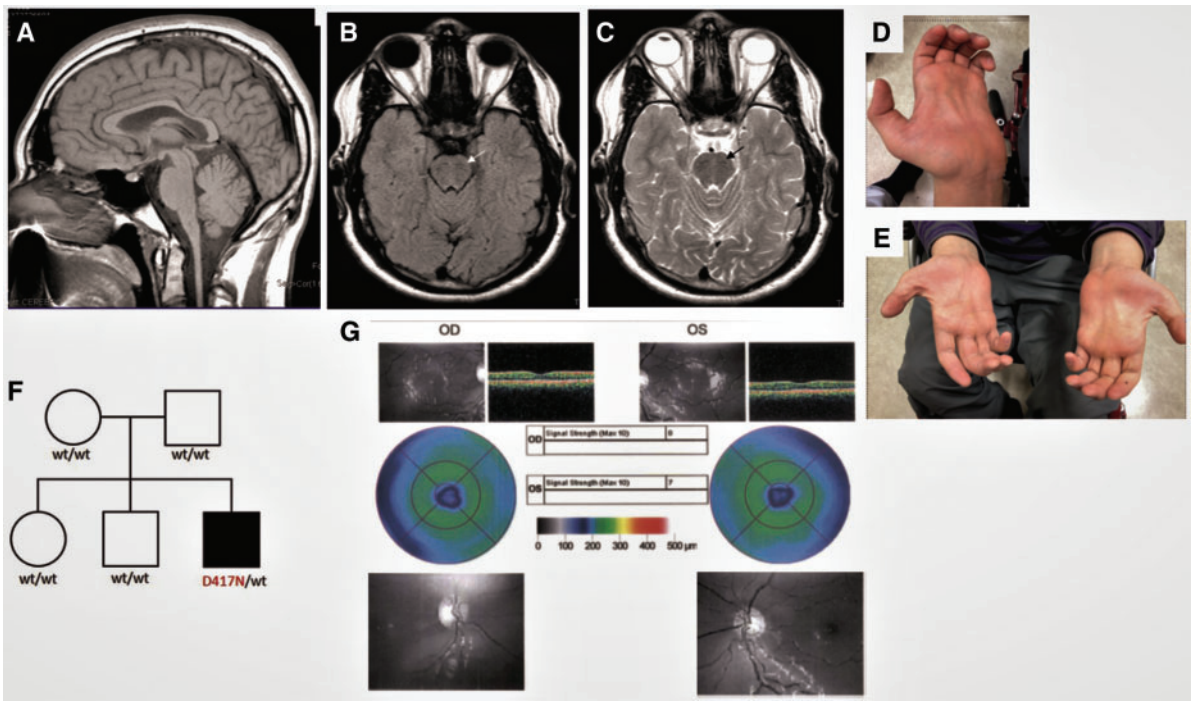

Figure 1. Clinical features of patient. (**A–C**) Brain MRI of patients at age 18 years. (A) T1 sagittal, notice atrophy of cerebellar vermis (superior anterior lobule); (B) Fluid attenuation inversion recovery (FLAIR) and (C) T2 weighted axial image. Arrows highlight the T2 and FLAIR hypointense stripes at the level of the pons. **D** and **E** show distal muscle atrophy of hands. **F** shows pedigree of family, the propositus corresponds to the black square filled in black. **G** shows OCT with normal parameters, while a bilateral temporal optic atrophy is evident bilaterally.

combined annotation dependent depletion (CADD) were prioritized on the basis of the functional relevance of genes, taking into account X-linked, autosomal dominant and autosomal recessive inheritance models, allowing identification of a *de novo* missense c.1249G>A (p.D417N) substitution in *TUBB2A* as the only excellent candidate. Sanger sequencing validated the variant and confirmed its *de novo* origin. Inspection of multiple sequence alignment including orthologs and paralogs showed that the residue is invariantly conserved (Fig. 5). The variant (or any other substitution affecting codon 417) had not previously been reported in public (123 000 exomes, gnomAD) and population-matched in-house (800 exomes) databases. The putative functional relevance of the p.D417N substitution was also predicted by different scores; including ExAC missense z score (6.2), residual variation intolerance score (Residual Variation Intolerance Score v4, −0.50) and gene damage index (2.41) (14), consistently indicating that TUBB2A is a protein intolerant to variation. Based on this finding, mutation analysis of the entire coding sequence of *TUBB2A* was performed in 14 *SACS* mutation-negative patients with symptoms suggestive of a sacsinopathy but did not identify any additional functionally relevant variants in this gene.

D417N does not affect the half-life of TUBB2A and its incorporation into microtubules

To determine the functional impact of p.D417N substitution and compare it with the p.A248V substitution that had previously been associated to both a non-progressive infantile-onset epilepsy with developmental brain abnormalities (11), and developmental delay with anterior temporal pachygyria (12), wild type (WT) and mutated C-terminally FLAG epitope (FLAG)-tagged *TUBB2A* constructs were generated and transfected into human embryonic kidney 293 (HEK-293) cells. We examined the impact of both p.D417N and p.A248V mutations on TUBB2A stability, evaluating the TUBB2A half-life upon inhibition of protein synthesis. Cells were transfected with WT and mutant constructs and after 24 h were treated with cycloheximide. The levels of TUBB2A in cell lysates were determined by western blotting.

Comparison of protein stability by cycloheximide treatment did not show significant difference in protein degradation among recombinant $TUBB2A^{WT}$ and $TUBB2A^{D417N}$, indicating that the p.D417N mutation does not significantly affect the short-term protein stability (Fig. 2). $TUBB2A^{A248V}$ instead was reduced to ∼16 and 18% after treatment with cycloheximide for 8 h and 12 h, respectively, compared with $TUBB2A^{WT}$. Interestingly, p.A248V was previously reported to impair the correct incorporation of TUBB2A into microtubule polymers of cultured cells (11).

To explore the effect of p.D417N on microtubules dynamics *in vitro*, HEK-293 cells transiently transfected to overexpress WT and mutant TUBB2A constructs were transferred to 4°C to induce microtubule depolymerization (30 min) and then to 37°C to promote cytoskeleton polymerization rescue. The ability of recombinant TUBB2A to assemble into microtubules was then evaluated in time-course experiments by immunofluorescence analysis.

A slower reintegration of $TUBB2A^{A248V}$ into microtubules as compared with WT TUBB2A (Fig. 3) was observed, consistent with the notion that p.A248V substitution affects TUBB2A incorporation into growing microtubules (11). Indeed, $TUBB2A^{A248V}$ incorporation appeared delayed during the early stages of repolymerization and microtubules polymerization rescue was completed only after 45 min (Fig. 3A and B). Differently from $TUBB2A^{A248V}$, $TUBB2A^{D417N}$ retained its ability to assemble into microtubule polymers, which appeared completely organized after 30 min. Interestingly, during microtubules regrowth a gradual accumulation of mitotic cells with aberrant spindle

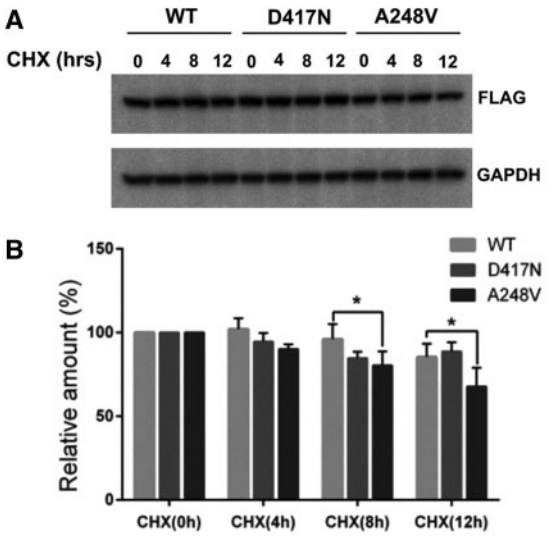

Figure 2. D417N substitution does not affect TUBB2A protein stability. (**A**) Western blot analysis of TUBB2A protein stability, performed on HEK-293 cells transiently transfected with FLAG-TUBB2A (WT and mutants) and treated with cycloheximide. GAPDH was used as a loading control. (**B**) Histogram shows the quantitative analysis for western blot. The relative levels before cycloheximide treatment (0 h) were set as 100%. The graph reports the mean ± SEM. $n = 3$ *$P < 0.05$.

occurred, suggesting that a high percentage of cells overexpressing the mutant TUBB2A^{D417N} was arrested in mitosis (Fig. 3A and C).

Immunocytochemical analysis showed normal colocalization of the recombinant TUBB2A^{D417N} with the endogenous α-tubulin in both transfected HEK-293 and HeLa cells (Fig. 4). Overall, these data indicate that, differently from what observed for TUBB2A^{A248V}, p.D417N mutation does not impair the incorporation TUBB2A into the microtubule network (Fig. 4, Supplementary Material, Fig. S1).

Structural analysis on the effects of the D417N variant of TUBB2A

Asp 417 is a solvent-exposed residue conserved invariant among TUBB2A orthologs and paralogs and located in a region that mediates binding to the motor domain of kinesins. Of note, this residue directly participates in such interaction (Fig. 5). The negatively charged Asp417 residue forms salt-bridges with the positively charged Arg307 and Arg316 residues in the motor domain of KIF1A, stabilizing the interaction with the kinesin. Both salt-bridges were predicted to be impaired by the Asp-to-Asn change, which introduces an uncharged residue. This observation strongly points to a weakened interaction with KIF1A as the mechanism underlying the functional effect of the TUBB2A^{D417N} mutant on the associated neurodegenerative disorder. In addition, we analyzed *in silico* the crystal structure of

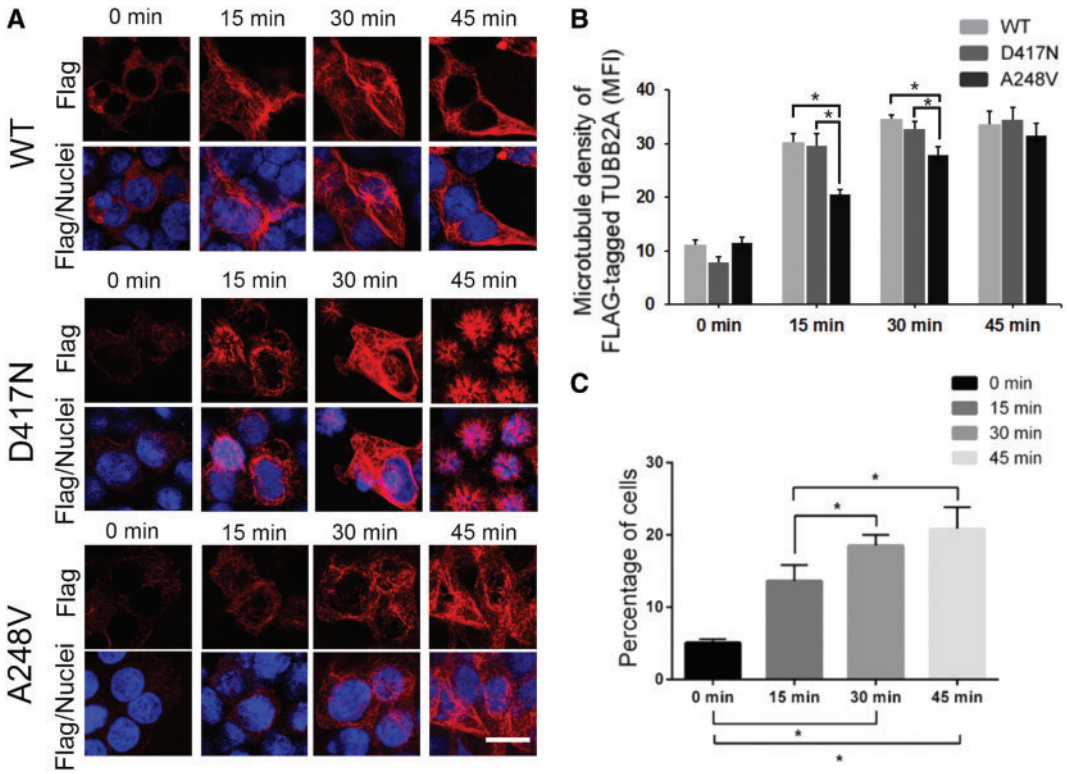

Figure 3. D417N substitution does not impair microtubule reassembly following cold-induced depolymerization. (**A**) HEK-293 cells overexpressing the recombinant TUBB2A (WT and mutants) were transferred to 4°C to induce the microtubule depolymerization and returned to 37°C promote microtubule reassembly. At defined time points, HEK-293 cells were analyzed by immunofluorescence experiments to visualize the rate of TUBB2A growth. Scale bar 20 μm. (**B**) Quantification of FLAG-tagged TUBB2A density was performed using ImageJ software. For each cell we quantify the FLAG-tagged TUBB2A staining relative to the area of the cell. The FLAG-tagged TUBB2A density was expressed as mean fluorescent intensity. Bars represent the means ± SEM. (**C**) Quantification of the effect of p.D417N on MI during TUBB2A regrowth. After ice cold treatment, HEK-293 cells overexpressing the recombinant TUBB2A (WT and mutants) were transferred to 37°C to promote microtubule reassembly and analyzed at defined points to evaluate the percentage of cells with abnormal mitotic spindle. Results are presented as mean ± SEM. $n = 3$ *$P < 0.005$.

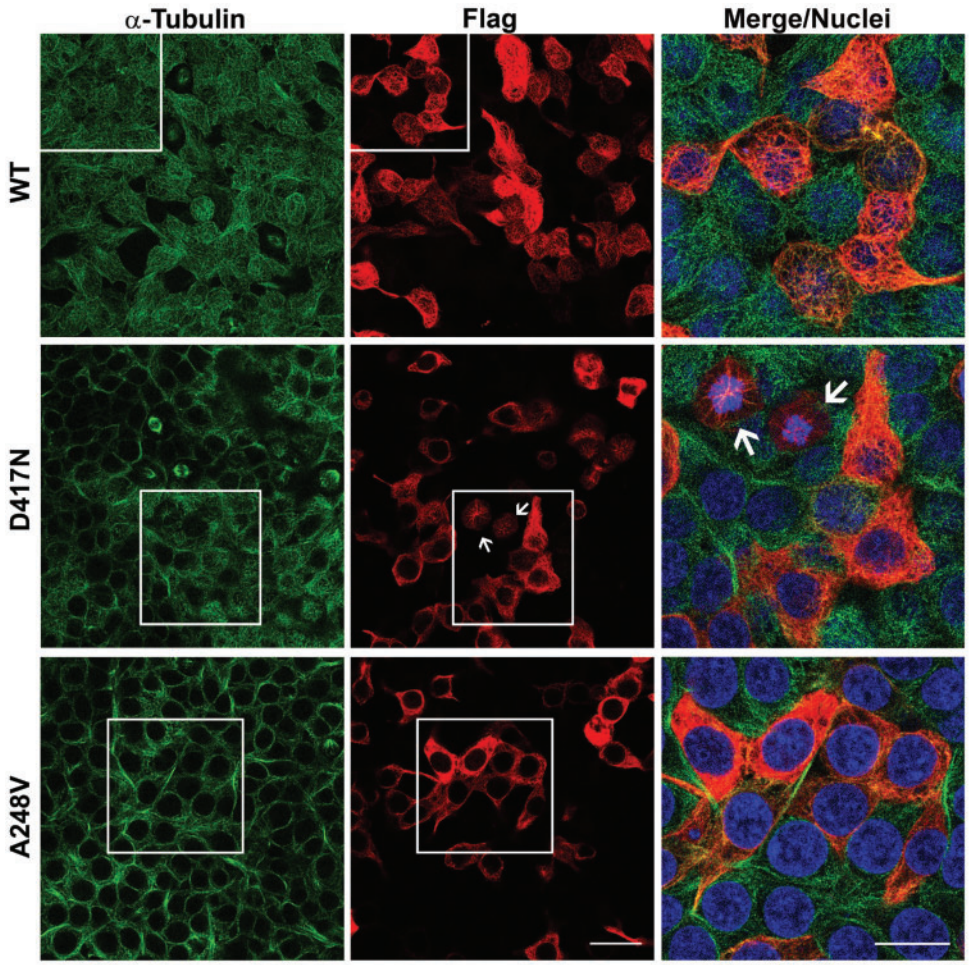

Figure 4. D417N variant and endogenous α-tubulin are normally incorporated into Microtubule Polymers *in vitro*. Immunofluorescence analysis of recombinant TUBB2A (WT and mutants) and endogenous α-tubulin in transfected HEK-293 cells. Scale bar 30 μm. High magnification of selected areas (white box) scale bar 20 μm.

apo-kinesin motor domains bound to α/β tubulin and found that additional kinesins show interfacial residues with highest similarity to those of KIF1A (Supplementary Material, Table S3).

Impact of D417N and A248V mutations on mitosis and spindle bipolarity

Microtubules play a crucial role during mitosis ensuring the correct mitotic spindle assembly and positioning and ensuring chromosome migration during anaphase.

We investigated the effect of p.D417N and p.A248V substitutions in TUBB2A on spindle assembly and mitosis in cultured HEK-293 cells transiently transfected with the mutant constructs. As shown, we observed that differently from the p.A248V mutation, the ectopic expression of p.D417N substitution caused the appearance of cells with misshapen spindle at the M phase (Fig. 6); in most cells the mitotic spindle had a monopolar structures with disorganized microtubules that extend from the cell pole toward the cell's periphery (Fig. 6A and C, Supplementary Material, Fig. S1). The number of cells presenting this phenotype correlated with the time of transfection suggesting that these abnormalities accumulate during replications (Fig. 6A and B).

A statistically increased mitotic index (MI) (i.e. the percentage of cells in mitosis) was documented in HEK-293 cells overexpressing the p.D417N mutation (42.8% for D417N mutation, versus 15.6 and 9.6% for A248V mutation and WT, respectively, at 48 h after transfection) (Fig. 6D). Prolonging the time of transfection, overexpression of TUBB2A^{D417N} was found to impair the balance of M phase entry and exit (MI = 42.8% at 48 h compared with 20.11% at 24 h) (Fig. 6B). Interestingly, after 48 h of transfection, recombinant TUBB2A^{D417N} and endogenous α-tubulin do not completely colocalize in microtubules of mitotic cells; the endogenous α-tubulin is located at the spindle pole within chromosomes while TUBB2A extend in an orientation opposite to that of the pole (Fig. 6A) indicating aberrant localization of the mutant protein possibly as a result of altered interaction with partner proteins. Therefore, HEK 293 cells overexpressing the p.D417N mutation showed a wide range of nuclear abnormalities, including defects in chromosome cohesion or attachment, at prometaphase (Fig. 6C).

Since its impact on microtubule dynamics, aberrant mitotic spindles were observed in HEK-293 cells overexpressing the p.A248V mutation, however, MI in these cells was much lower as compared with those overexpressing the p.D417N substitution (Fig. 6D).

Abnormalities in mitotic spindle are visible also in HeLa cells transiently transfected with the TUBB2A^{D417N} mutant but with a much lower frequency probably due to the lower replicative activity (Supplementary Material, Fig. S1). Of note, cells overexpressing the TUBB2A^{D417N} mutant inducing mitosis show

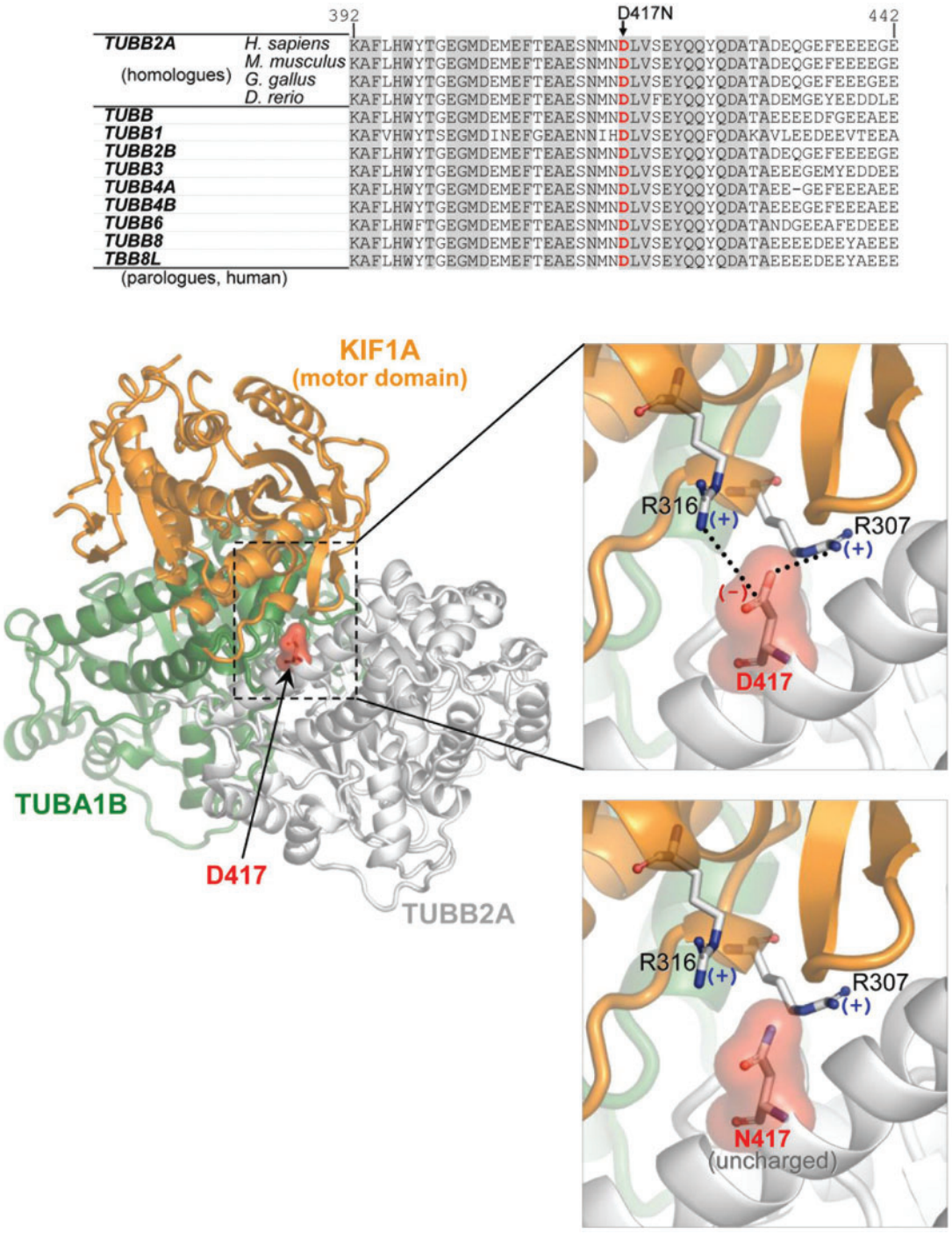

Figure 5. *In silico* structural analysis and alignment of the D417N amino acid change. Multiple sequence alignment of the TUBB2A protein around the site affected by the disease-causing D417N amino acid change (invariant residues are grayed), and homology model of the complex of the human TUBB2A protein (showing the site of the D417 mutation) with TUBA1B, and the KIF1A motor domain. The WT inset highlights D417 and the salt-bridges (dotted lines) formed with the arginines R307 and R316 in the motor domain of KIF1A. The mutant inset represents a modeled D417N amino acid replacement.

multipolar spindles as the predominant mitotic structures together with monopolar spindles: in these cells, microtubules appeared generally thick and preferentially located at one side of the cell. Moreover, in these structures, exogenous TUBB2A^{D417N} and endogenous α-tubulin exhibited only partial colocalization; with the former extending toward the poles to cell periphery and the latter been located only in proximity of the nuclei. (Supplementary Material, Fig. S1). These data strongly suggest that the D417N mutation in TUBB2A disrupts the spindle bipolarity, resulting in a delay of cell to exit from the M phase and increasing the percentage of mitotic cells.

Interestingly, p.D417N substitution had previously been reported in TUBB8, a highly homologous β-tubulin isoform expressed during human oocyte development, and was

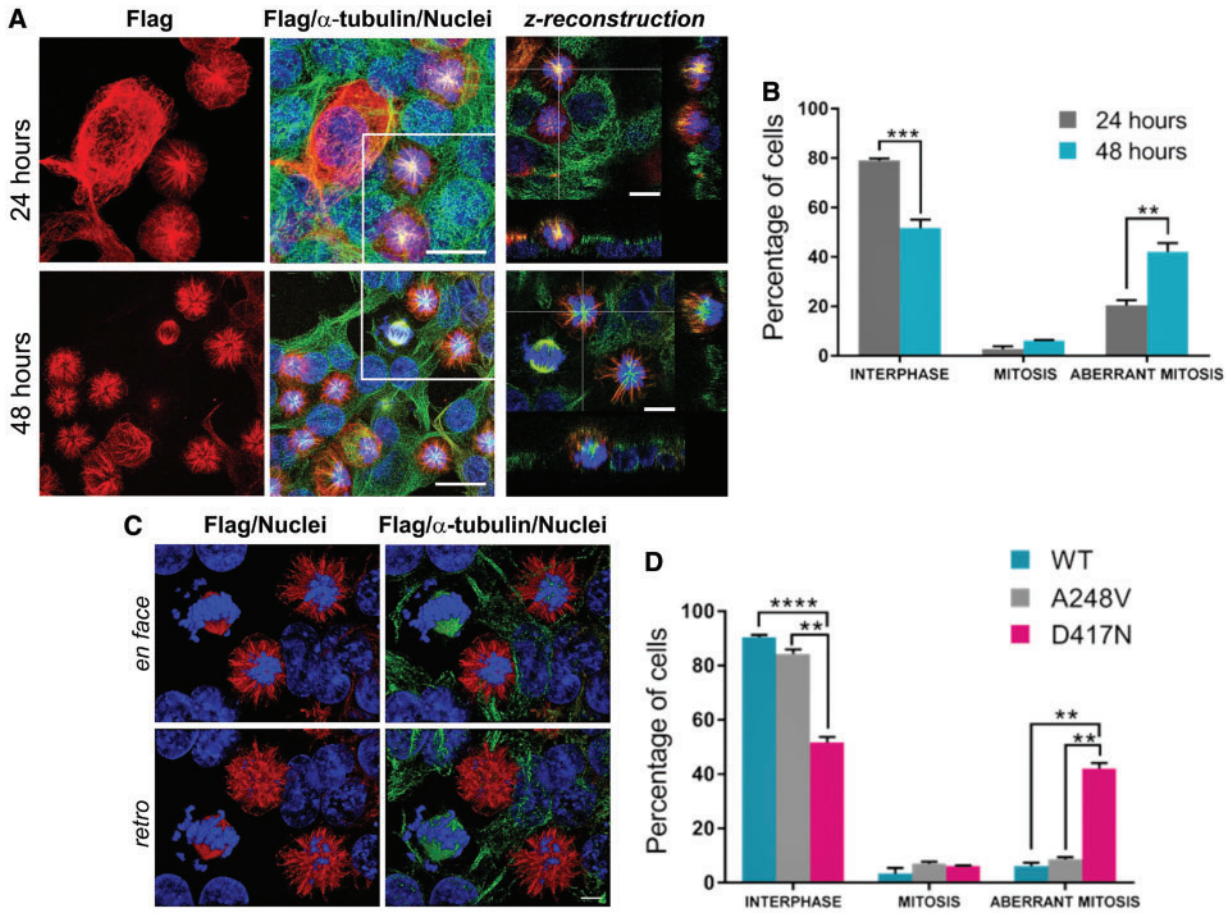

Figure 6. D417N substitution in TUBB2A impairs bipolar spindle formation causing mitotic arrest. (**A–C**) Immunofluorescence analysis of the mutant TUBB2A harboring the p.D417N substitution in HEK-293 cells transiently transfected for 24 and 48 h. Scale bar 5 μm. (B) Quantification of the effect of p.D417N on MI after 24 or 48 h of transfection. Results are presented as mean ± SEM. $n = 3$ $^{**}P < 0.005$, $^{****}P < 0.0001$. (C) 3D reconstruction of the insert in A showing the frontal face image (*en face*) and the rear face image (*retro*). (**D**) Quantification of the effect of p.D417N and p.A248V mutations on MI. Results are presented as mean ± SEM. $n = 4$ $^{**}P < 0.005$, $^{****}P < 0.0001$.

documented to impair the proper spindle formation resulting in meiotic arrest in both mouse and human oocytes (15). To better evaluate the impact of p.D417N on cell cycle progression and microtubule spindle organization, HeLa cells transiently transfected with WT or mutant TUBB2A proteins were synchronized at G1/S boundary by thymidine-nocodazole treatment. At metaphase, HeLa cells overexpressing the p.D417N substitution showed aberrant spindle morphology. Mitotic spindle originated from multiple cellular points and presented supernumerary pericentrin spots indicating a dramatic disruptive impact on proper chromosomal segregation and cell division (Supplementary Material, Fig. S2).

Impact on microtubule stability in primary fibroblast of patient harboring the D417N variant1

TUBB2A is a major tubulin subtype in neurons but is also expressed at lower levels in other cell lineages (10). We evaluated the levels of TUBB2A in primary fibroblasts in comparison with other major β-tubulin isotypes (TUBB, TUBB2C, TUBB2B, TUBB3, TUBB4, TUBB1 and TUBB6). We observed that TUBB (class I) and TUBB2C (class IVb) were the most expressed β-tubulin isotypes representing the 60 and 22%, respectively, of the total β-tubulin content in fibroblasts. TUBB6 (class V) and TUBB3 (class III) were discreetly expressed, while TUBB2A (class IIa) was very lowly expressed (3%). TUBB2B (class IIb), TUBB4 (class IVa) and TUBB1 (class VI) instead were not expressed (Fig. 7).

Although the percentage of TUBB2A expression in fibroblasts was rather low, since the dramatic effect of p.D417N mutation on spindle formation and mitosis, we evaluated the impact of the mutation in primary fibroblasts obtained from of the affected patient. Control and mutant fibroblasts were synchronized at G1/S boundary by thymidine-nocodazole and after G1/S release, we evaluated the progression of mitosis by time-course experiments. Consistent with our findings, on transfected cells, p.D417N affected the spindle morphology and chromosome condensation; cells predominantly showed monopolar spindles that during cytokinesis unequally distributed chromosomes to multiple daughter cells (Fig. 8).

Comparative analysis of KIF1A affinity to TUBB2A^{D417N} and TUBB2A^{A248V}

In the microtubule–kinesin complex, Asp417 is located at the residue has been previously reported to be located at the inter domain interface between microtubules and kinesin superfamily motor proteins and has been reported to be critical for binding of kinesin to the microtubule (16,17).

Mutation affecting the Asp417 residue previously reported in TUBB3 (NM_006086.3), a neuron-specific β-tubulin isoform showing

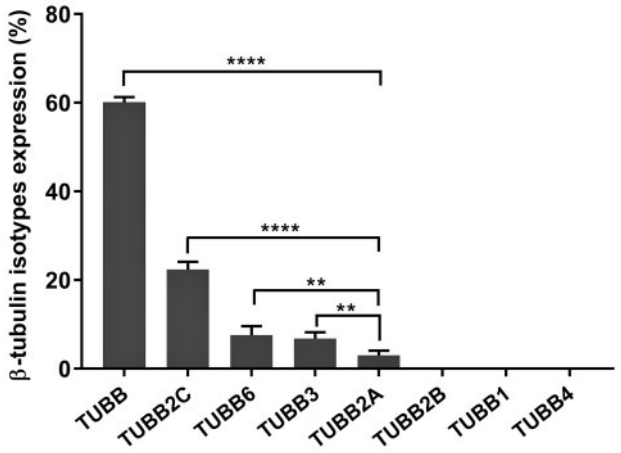

Figure 7. Expression of β-tubulin isotypes in human primary fibroblasts detected by RT PCR. Real-time analysis of β-tubulin isotypes conducted on primary fibroblasts of healthy individuals ($n = 4$). Expression values were normalized to GAPDH expression. Results are presented as mean ± SEM. $n = 4$ $^{**}P < 0.005$, $^{****}P < 0.0001$.

92% amino acid sequence identity to TUBB2A, perturbs the binding of kinesins to microtubules in cultured cells (18–19), impairing axonal transport (18). Consistent with such a critical role, substitutions affecting this residue (p.D417H and p.D417N) have been found in patients with an early-onset neurological syndrome with ophthalmoparesis and progressive peripheral neuropathy (20).

Kinesins are important molecular motors that directionally transport cargos including proteins, organelles and mRNA by moving along microtubules (20). They have a central role in neuronal function, plasticity and morphogenesis by transporting synaptic vesicle precursors, neurotransmitter and neurotrophic factor within axons, dendrites and synapses (21).

In addition to their role of intracellular transporters, kinesins participate in chromosome attachment during cell division and contribute to anaphase spindle elongation, ensuring proper segregation of chromosomes between daughter cells to avoid aneuploidy (22).

Since the specific impact of the TUBB2A^{D417N} mutant on mitotic spindle structure, we investigated the *in vitro* association of WT and mutants TUBB2A with the kinesin KIF1A, by performing coimmunoprecipitation assays on lysates from HEK-293 transiently transfected with FLAG-tagged TUBB2A constructs.

As shown in Figure 9, recombinant TUBB2A^{WT} coimmunoprecipitated with the endogenous KIF1A in adenosine triphosphate-devoid condition. Consistent with the *in silico* predictive modeling, the p.D417N change strongly reduced the affinity of TUBB2A for kinesin (Fig. 9).

Although TUBB2A^{A248V} coimmunoprecipitated less with the endogenous KIF1A, considering that the p.A248V has been reported to perturb the incorporation of TUBB2A into microtubules increasing the portion of unpolymerized TUBB2A, the variability observed in TUBB2A-KIF1A affinity could be explained not by a low binding affinity of TUBB2A^{A248V} to KIF1A but rather by a reduced pool of TUBB2A incorporated into microtubule polymers that coimmunoprecipitate with KIF1A.

Discussion

Tubulinopathies constitute a wide family of neurodevelopmental disorders characterized by an overlapping range of brain

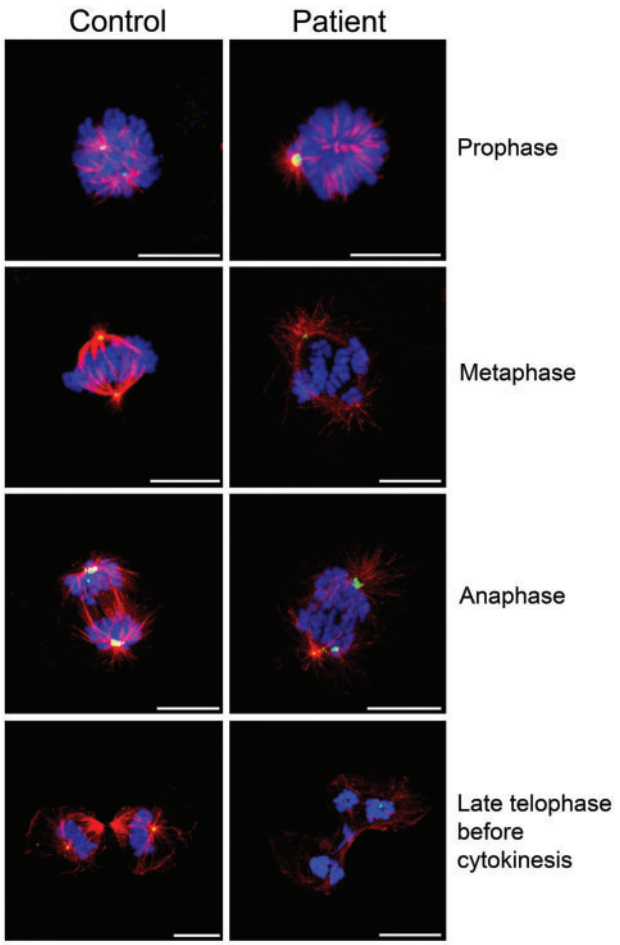

Figure 8. D417N substitution affects Mitotic Spindle and chromosomes condensation in fibroblasts. Immunofluorescence analysis of synchronized skin fibroblasts of healthy individuals and the patient harboring the p.D417N substitution. Cells were stained using antibodies against pericentrin (green, centrosome marker) and α-tubulin (red, marker for microtubules and mitotic spindle); chromosomes are 4',6-diamidino-2-phenylindole stained (blue). Scale bars represent 10 μm.

malformations caused by mutations in genes encoding for different isotypes of α and β-tubulins, the structural components of microtubules (23). In this study, we report on a previously unreported dominantly acting missense mutation, p.D417N, in TUBB2A, one of the neuron-specific β-tubulin isotype II family, resulting in a progressive neurological condition of spastic paraplegia, peripheral sensory motor neuropathy and ataxia. Interestingly, the equivalent amino acid change had previously been reported in TUBB3 and has been associated with a progressive early-onset peripheral neuropathy showing a very similar brain abnormality to the present phenotype consisting in hypoplasia of the posterior body of the corpus callosum (20).

We investigated the pathogenic role of the disease-associated mutation and provide evidence that p.D417N substitution disrupts the dynamics of mitotic spindle and mitosis.

In cells expressing the TUBB2A^{D417N} mutant the MI was drastically increased. These cells showed monopolar and multipolar spindle with altered α/β tubulin colocalization and presented a wide range of nuclear abnormalities including defects in chromosome cohesion or attachment. Consistent with these findings, in primary fibroblasts, although the expression of the TUBB2A variant was rather low compared with the major

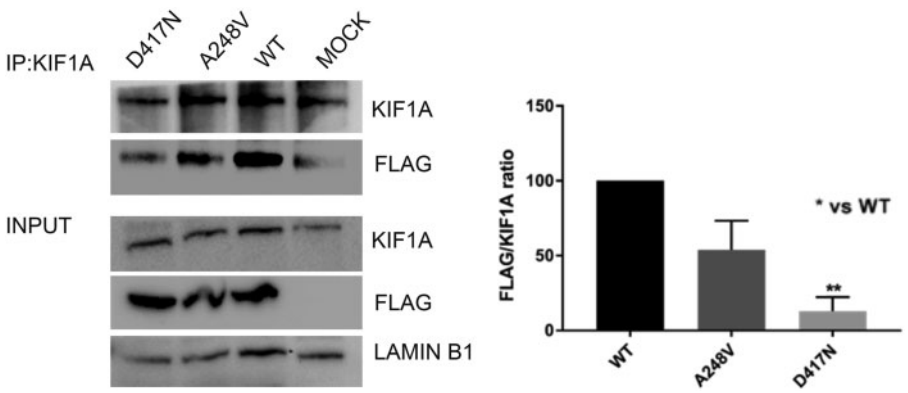

Figure 9. D417N substitution affects the TUBB2A binding to kinesin KIF1A. Coimmunoprecipitation assay was used to detect the interaction between the endogenous KIF1A and recombinant TUBB2A (WT and mutants). The graph reports the mean ± SEM. $n = 3$ **$P < 0.005$. Results are expressed as percentage of control (=100).

β-tubulin isotypes, the p.D417N substitution caused similar abnormalities in spindle morphology; fibroblasts predominantly showed aberrant monopolar spindles that during cytokinesis unequally distributed chromosomes to multiple daughter cells. In agreement with the present findings, the equivalent substitution reported in the TUBB8, which is a highly homologous β-tubulin isoform expressed during human oocyte development, has been reported to impair the correct spindle formation resulting in a meiotic arrest in both mouse and human oocytes (15).

Cell cycle defects and associated aneuploidy have been described in several neurodegenerative disorders (24–27); however, their impact in neurodegeneration remains poorly understood. Fibroblasts derived from patients affected by Huntington's disease and from R6/2 transgenic mice, the most widely used model to study Huntington's disease, showed a high frequency of multiple centrosomes and aneuploidy (28) and individuals affected by Alzheimer's disease (AD) showed increased aneuploidy in brain as well as in peripheral cells (29–31): aneuploid neurons in AD patients are particularly prone to degeneration and could account for 90% of the neuronal loss that occurs in the late-stage of this pathology (32,33).

Considering the late-onset slowly progressive neurodegeneration observed in our patient harboring the p.D417N mutation, it is highly suggestive to hypothesize that the defective mitoses associated to p.D417N in TUBB2A may promote aneuploidies in postmitotic neurons and glial cells that might contribute to neurodegeneration. TUBB2A has in fact reported to be a neuronal-specific β-tubulin isotype, showing a much lower expression in other human tissues (10). Considering its specific neuronal expression, it is likely that *TUBB2A* may be particularly expressed in neuronal progenitor and its expression increases mainly during neuronal differentiation when neuronal progenitor still retain their ability to undergo mitosis and this could explaining why defective mitoses associated to p.D417N mutation mainly affect neurons rather other cell types.

Of note, it has been demonstrated that the highly conserved Asp417 residue is located at the interface between microtubules and kinesin superfamily motor proteins and that it is critical for the binding of kinesin to the microtubule. In particular, the negatively charged Asp417 residue interacts with the positively charged Arg307 and Arg316 residues in the motor domain of KIF1A (Fig. 5), a neuron-specific kinesin motor required for the transport of synaptic vesicle precursors (34), stabilizing the interaction with the kinesin. Our *in silico* predicting and *in vitro data* support the idea that the p.D417N mutation, that substitutes the negatively charged Asp with the uncharged Asn, affects the binding of TUBB2A with the Arg 307 and Arg 316 residues of KIF1A (Fig. 5). Similarly, the mutations R307Q and R316W in the motor domain of KIF1A, that substitute the positively charged Arg with the uncharged residues Gln and Trp were predicted to impair the binding of KIF1A to microtubules (35,36) and are associated with complex neurologic phenotypes characterized by cognitive impairment, optic nerve atrophy, cerebellar atrophy, spasticity (36) and peripheral neuropathy (35) that overlap with the phenotype observed in the patient harboring the p.D417N substitution in TUBB2A. Moreover, additional mutations in KIF1A were associated to degenerative neurological conditions with a progressive course (37,38) and *Kif1a* mutant mice exhibit a neurodegenerative phenotype characterized by severe motor and sensory disturbances (39). Hippocampal neurons of *Kif1a* mutant mice mature and establish mature synapses *in vitro*, however, at 8 days in culture when the level of *Kif1a* expression in WT mice increases, they showed neurite fragmentation and cell body condensation and are prone to degeneration that definitively occurs at 13 days in culture (39).

Considering the critical role of KIF1A in the maintenance and function of mature neurons, loss of binding of TUBB2A to KIF1A in neurons, could impair the axonal transport disrupting neuronal function and resulting in a gradual neuronal cell death contributing to a progressive neurodegenerative process as in our patient.

Mutations affecting the Asp417 residue were previously described in TUBB3 (NM_006086.3) (20), a neuron-specific β-tubulin isoform showing 92% amino acid sequence identity to TUBB2A, and were reported to perturb microtubule affinity for kinesins and kinesin-dependent axonal transport (18). In particular, Niwa *et al.* (18) have demonstrated that the p.D417H substitution in TUBB3 perturbs the binding of kinesins and the axonal transport of mitochondria when expressed in cultured mammalian neurons. In addition, they have showed that the pathogenic effect of the p.D417H mutation is independent of the tubulin isoform and that the overexpression of $TUBB2^{D417H}$ or $TUBB5^{D417H}$ mutants similarly inhibited the axonal transport. Likewise, studies conducted in budding yeast have showed that p.D417H and p.D417N substitutions perturbed the kinesin-microtubule interaction resulting in a loss of kinesin localization on microtubule plus-ends (20). The Asp^{417} residue is evolutionarily conserved across β-tubulin isotypes (Fig. 5) and both p.D417N and p.D417H mutations introduce an uncharged Asn or a positively charged His instead of the negatively charged Asp (18,20)

demonstrating that the Asp417 residue is critical in mediating microtubule–kinesin interaction and axonal transport. Based on these evidences, we strongly hypothesize that mutations affecting the Asp417 residue in β-tubulin isotypes reduce microtubule affinity for kinesins impairing kinesin-dependent transport and that the TUBB2A^{D417N} mutant may act with a similar pathogenic mechanism to that of TUBB3^{D417H} and TUBB3^{D417N} mutants.

Consistent with what has been previously reported, p.D417H and p.D417N mutations in TUBB3 induce in humans severe neurological symptoms, such as progressive peripheral neuropathy and loss of axons (18–20).

As anticipated, the growing evidence in AD of an impairment of mitotic spindle formation and the generation of aneuploidy is also a consequence of the excess of Tau protein that disrupts the interaction between specific kinesins and microtubules (40,41). In fact, kinesin performs a variety of functions during cell division, and within the mitotic spindle to ensure that chromosomes are correctly segregated (42,43) and defects in kinesin proteins have been shown to affect the spindle assembly and cell cycle progression (44–49). Based on these evidences, we cannot exclude that the p.D417N mutation, in addition to KIF1A, may impair the binding with additional kinesins, and that the effect of the p.D417N mutation on mitosis could occur via the dysfunction of these motor proteins. The interfacial residues of KIF1A motor domain are in fact highly conserved in kinesins KIF1B and KIF1C (Supplementary Material, Table S3) suggesting that the p.D417N mutation in TUBB2A could affect the microtubule binding of these additional kinesins.

Interestingly, *Kif1b* heterozygous mice suffer of a late-onset axonopathy similar to the Charcot-Marie-Tooth disease type IIA (CMT2A) and in humans the missense mutation Q98L mutation in *KIF1B* is associated with the autosomal dominant CMT2A (50). Similarly, mutations in *KIF1C* were described in patients with spastic paraparesis and cerebellar dysfuntion (51,52).

Differently from the p.D417N substitution, the p.A248V variant identified in patients with neurodevelopmental disease, affects a conserved residue of TUBB2A located in the T7 loop positioned at the interface between the α–β tubulin heterodimer and involved in the guanosine triphosphate bound to the α-subunit. From this, it follows that this mutation impairs the ability of incorporation into microtubules, without drastically affecting neither the binding of TUBB2A to KIF1A nor mitotic spindle bipolarity as we observed for the D417N substitution.

In conclusion, our comparative analysis of p.D417N substitution with p.A248V shows different pathogenic mechanisms associated to the p.D417N variant explaining the difference in the genotype phenotype correlation.

Overall, this study associates a novel mutation in *TUBB2A* with a neurodegenerative phenotype extending the phenotypic spectrum of β-tubulin 2A beyond a phenotype of developmental brain malformation and infantile-onset epilepsy.

Materials and Methods

Whole exome sequencing

WES was conducted on the proband, his parents and two unaffected siblings using genomic DNA extracted from leukocytes after informed signed consents was secured. Exome regions were enriched with SureSelect Human All Exon v4 kit (Agilent Technologies), and sequencing was performed on a platform (Illumina). WES data were processed using an in-house implemented pipeline as previously reported (53–55). Sequencing output is summarized in Supplementary Material, Table S1. High-quality variants were annotated and considered for successive steps if having not been reported or having a minor allele frequency < 0.001 in genome AD exomes database (56), and occurring with a frequency < 0.01 in our in-house database (~900 exomes). Variants of the proband were filtered to retain all non-synonymous changes and intronic variants adjacent to splice sites (−3/+8). Functional annotation of variants was performed using SnpEff v4.3 and dbNSFP v3.5 (57,58) and their functional impact was analyzed by CADD (v.1.3) (59). The *TUBB2A* c.1249G>A variant reported in this study was submitted into the Leiden Open Variation Database (www.LOVD.nl/TUBB2A; patient ID 00146422).

Plasmid constructs

Flag-tagged TUBB2A expression vector was generated by polymerase chain reaction (PCR) amplification of reverse-transcribed RNA isolated from human primary fibroblasts using a specific primer annealing at the 5′ region with an artificial *Eco*RI site overlapping the start codon and a specific primer annealing at the 3′ regions overlapping the stop codon and containing the sequence for the FLAG tag with an artificial site *NotI*. After *Eco*RI and *NotI* digestion, the full length coding region of TUBB2A was cloned into pCDNA3.1 vector (Invitrogen) and the single-nucleotide changes resulting in the p.D417N and p.A248V substitutions were introduced by site-directed mutagenesis (Stratagene, UK). The entire transgene-coding regions were sequence validated following maxiprep yields (QIAgen).

Protein stability assay

Hek-293 cells were transiently transfected using 0.5 μg of WT and mutant TUBB2A constructs and after 24 h of transfection treated with 10 μg/ml cycloheximide at 37°C to block protein synthesis. At defined time points, cells were washed twice with PBS and lysed on ice with Radioimmunoprecipitation assay buffer (50 mM Tris–HCl, pH 7.4, 50 mM NaCl, 0.1% sodium deoxycholate, 1% Triton, 0.5% sodium deoxycholate including phosphatases and protease inhibitors) on ice for 10 min. Cell debris was removed by centrifugation at 12 000*g* at 4°C for 15 min and protein level of TUBB2A was detected by western blotting.

Cell culture and reagents

HEK293 data about HeLa are in Supplemental Materials, exclude here and skin fibroblast cells were cultured in Dulbecco's modified Eagle's medium (DMEM, Sigma) supplemented with 10% fetal bovine serum (Sigma), 2 mM L-glutamine and 1% penicillin/streptomycin solution at 37°C.

Transient cell transfection and immunofluorescence

HEK-293 were seeded in 6-well plates and after overnight incubation transfected Flag-tagged *TUBB2A* expression vectors using Lipofectamine 2000 (Invitrogen Life Technologies). In total, 24 or 48 h after transfection, cells were fixed with ice–cold methanol for 7 min, blocked with 5% bovine serum albumin for 1 h and subsequently incubated with the indicated primary antibodies: mouse anti-FLAG (1:500, 1 h, Sigma-Aldrich), rabbit anti-α tubulin (1:250, 2 h, Sigma).

Confocal microscopy was performed on a Leica TCS-SP8X laser-scanning confocal microscope (Leica Microsystems, Mannheim,

Germany) equipped with white light laser source and 405 nm diode laser. Sequential confocal images were acquired using a HC PLAPO 63x oil immersion objective (1.40 numerical aperture, Leica Microsystems) with a 1024 × 1024 format, scan speed 400 Hz and z-step size of 0.3 μm. z-reconstructions were imported into LAS X 3D Analysis (Leica Microsystems) software to obtain their three-dimensional (3D) surface rendering.

Fibroblasts synchronization and immunofluorescence

Fibroblasts were seeded in 24-well cluster plates onto 12 mm cover glasses. After 24 h of culture in complete medium cells were treated with 2 mM Thymidine (Sigma) for 24 h, washed with PBS 1X and then treated with 100 ng/ml nocodazole (Sigma) for 12 h. Afterwards, fresh drug-free medium was added to recovery and cells were fixed every 15 min using PHEMO buffer for 10 min at room temperature. Finally, cells were stained with anti-pericentrin (Abcam) and anti-α tubulin (Abcam), antibodies.

Observations were performed on a Leica TCS SP2 AOBS apparatus (Leica Microsystems) by the confocal software, using the 63x/1.4 NA oil objective and excitation spectral laser lines at 488, 594 and 633 nm. Cells stained only with the fluorochrome-conjugated secondary antibodies were used to set up acquisition parameters. Signals from different fluorescent probes were taken in sequential scanning mode, several fields (>200) were analyzed for each labeling condition, and representative results are shown.

Coimmunoprecipitation experiments

HEK-293 cells were transiently transfected with WT and mutant TUBB2A and after 48 h of transfection were lysate in 500 μl of lysis buffer containing 50 mM Tris–HCl pH 7.5, 150 mM NaCl, 1 mM ethylenediaminetetraacetic acid, 1% Triton and phosphatase and protease inhibitors. Five hundred micrograms of proteins were incubated for 1 h at 4°C with 20 μl of recombinant protein A/G agarore (Santa Cruz) to minimize non-specific binding. After centrifugation, 2 μg of Kif1A polyclonal antibody or 2 μg of Rabbit polyclonal IgG was added to the lysate, and samples were rotated for 1 h at 4°C. Thirty microliters of recombinant protein A/G-agarose gel were then added, and incubation was continued for 2 h at 4°C. Beads were washed six times with 500 μl of lysis buffer. After washing, samples were subjected to sodium dodecyl sulphate polyacrylamide gel electrophoresis, transferred to a polyvinylidene fluoride membrane and immunoblotted with the following primary antibodies: FLAG (1:2000, Sigma-Aldrich), KIF1A (1:2000, Abcam, Cambridge, UK) and LamB1 (1:1000, SantaCruz).

Quantitative real-time PCR

Total mRNA from primary fibroblasts of healthy individuals was isolated using Trizol Reagent (Sigma-Aldrich), according to the manufacturer's protocol. One micrograms of each RNA samples was reverse transcribed with the SuperScript First-Strand Synthesis system and random hexamers as primers (Life Technologies, Carlsbad, CA, USA). The expression levels of TUBB2A, TUBB, TUBB2C, TUBB2B, TUBB3, TUBB4, TUBB1 and TUBB6 were measured by quantitative real-time PCR (qRT-PCR) in an ABI PRISM 7500 Sequence Detection System (Life Technologies) using Power SYBR Green I dye chemistry. Data were analyzed using the 2-Delta-Delta Ct method with glyceraldehyde 3-phosphate dehydrogenase (GAPDH) as housekeeping gene and data are shown as fold change relative to control. Notably, the use of an alternative housekeeping gene such as the glucuronidase beta gene did not modified the data obtained with GAPDH gene.

Homology modeling of the human tubulin beta-2A chain

The human tubulin beta-2A chain (TUBB2A) was built by homology modeling as a complex with the tubulin alpha-1B chain (TUBA1B) and the KIF1A motor domain using the Protein Data Bank (PDB) entry 4LNU (containing a tubulin/kinesin motor domain complex) as the template. In the modeled ranges, residues 1–431 for TUBB2A, 1–437 for TUBA1B and 5–352 for KIF1A, these proteins share 98, 99 and 39% amino acid identity with their respective homologs in the template crystal structure.

The following modeling procedure was employed. In each monomer of the template, the side chain atoms were removed, and the remaining backbone atom-only residues were renamed and renumbered (in PDB format) to the corresponding amino acids of their homologs (human TUBB2A, TUBA1B and KIF1A proteins) according to sequence alignments shown in Supplementary Material, Table S2. The backbone-only structure was parsed to SIDEpro—(60)—for construction of side chains. The modeled monomers were maintained in same poses as their homologs in the template structure to reproduce the trimeric quaternary structure.

Data analysis and statistics

Statistical analysis was performed using the GRAPHPAD/Prism 7.0 Software (SanDiego, CA, USA). Statistically significant differences between groups were analyzed using Student's *t*-test for normally distributed variables. All data are presented as mean ± standard error of the mean (SEM). Statistical significance was defined as $^{*}P < 0.05$, $^{**}P < 0.005$, $^{****}P < 0.0001$.

Supplementary Material

Supplementary Material is available at *HMG* online.

Conflict of Interest statement. The corresponding author on behalf of all the coauthors confirms that there are there are no conflicts of interest to declare by all the authors. In particular the corresponding author, on behalf of all the coauthors, declares that there are no financial interests or connections, direct or indirect or other situations that might raise the question of bias in the work reported or the conclusions, implications or opinions stated—including pertinent commercial or other sources of funding for the individual author(s) or for the associated department(s) or organization(s), personal relationships or direct academic competition.

Funding

This work was supported in part by grants from Fondazione Bambino Gesù (Vite Coraggiose to M.T.); Ministero della Salute (RC2016 and RC2017 to M.T. and E.B.).

References

1. Gierke, S., Praveen Kumar, P. and Torsten Wittmann, T. (2010) Analysis of microtubule polymerization dynamics in live cells. *Methods Cell Biol.*, **97**, 15–33.

2. Breuss, M. and Keays, D.A. (2014) Microtubules and neurodevelopmental disease: the movers and the makers. *Adv. Exp. Med. Biol.*, **800**, 75–96.
3. Kapitein, L.C. and Hoogenraad, C.C. (2015) Building the neuronal microtubule cytoskeleton. *Neuron*, **87**, 492–506.
4. Smith, B.N., Ticozzi, N., Fallini, C., Gkazi, A.S., Topp, S., Kenna, K.P., Scotter, E.L., Kost, J., Keagle, P., Miller, J.W. *et al.* (2014) Exome-wide rare variant analysis identifies TUBA4A mutations associated with familial ALS. *Neuron*, **84**, 324–331.
5. Lopata, M.A. and Cleveland, D.W. (1987) In vivo microtubules are copolymers of available beta-tubulin isotypes: localization of each of six vertebrate beta-tubulin isotypes using polyclonal antibodies elicited by synthetic peptide antigens. *J. Cell Biol.*, **105**, 1707–1720.
6. Ludueña, R.F. (1998) Multiple forms of tubulin: different gene products and covalent modifications. *Int. Rev. Cytol.*, **178**, 207–275.
7. Sullivan, K.F. and Cleveland, D.W. (1986) Identification of conserved isotype-defining variable region sequences for four vertebrate beta tubulin polypeptide classes. *Proc. Natl. Acad. Sci. U. S. A.*, **83**, 4327–4331.
8. Cleveland, D.W. (1987) The multitubulin hypothesis revisited: what have we learned? *J. Cell Biol.*, **104**, 381–383.
9. Joshi, H.C. and Cleveland, D.W. (1989) Differential utilization of beta-tubulin isotypes in differentiating neurites. *J. Cell Biol.*, **109**, 663–673.
10. Leandro-García, L.J., Leskelä, S., Landa, I., Montero-Conde, C., López-Jiménez, E., Letón, R., Cascón, A., Robledo, M. and Rodríguez-Antona, C. (2010) Tumoral and tissue-specific expression of the major human beta-tubulin isotypes. *Cytoskeleton*, **67**, 214–223.
11. Cushion, T.D., Paciorkowski, A.R., Pilz, D.T., Mullins, J.G., Seltzer, L.E., Marion, R.W., Tuttle, E., Ghoneim, D., Christian, S.L., Chung, S.K. *et al.* (2014) De novo mutations in the beta-tubulin gene TUBB2A cause simplified gyral patterning and infantile-onset epilepsy. *Am. J. Hum. Genet.*, **94**, 634–641.
12. Rodan, L.H., El Achkar, C.M., Berry, G.T., Poduri, A., Prabhu, S.P., Yang, E. and Anselm, I. (2017) De novo TUBB2A variant presenting with anterior temporal pachygyria. *J. Child Neurol.*, **32**, 127–131.
13. Ejaz, R., Lionel, A.C., Blaser, S., Walker, S., Scherer, S.W., Babul-Hirji, R., Marshall, CR., Stavropoulos, D.J. and Chitayat, D. (2017) De novo pathogenic variant in TUBB2A presenting with arthrogryposis multiplex congenita, brain abnormalities, and severe developmental delay. *Am. J. Med. Genet. A*, **173**, 2725–2730.
14. Itan, Y., Shang, L., Boisson, B., Patin, E., Bolze, A., Moncada-Vélez, M., Scott, E., Ciancanelli, M.J., Lafaille, F.G., Markle, J.G. *et al.* (2015) The human gene damage index as a gene-level approach to prioritizing exome variants. *Proc. Natl. Acad. Sci. U. S. A.*, **112**, 13615–13620.
15. Feng, R., Sang, Q., Kuang, Y., Sun, X., Yan, Z., Zhang, S., Shi, J., Tian, G., Luchniak, A., Fukuda, Y., Li, B. *et al.* (2016) Mutations in TUBB8 and human oocyte meiotic arrest. *N. Engl. J. Med.*, **374**, 223–232.
16. Uchimura, S., Oguchi, Y., Katsuki, M., Usui, T., Osada, H., Nikawa, J., Ishiwata, S. and Muto, E. (2006) Identification of a strong binding site for kinesin on the microtubule using mutant analysis of tubulin. *EMBO J.*, **25**, 5932–5941.
17. Uchimura, S., Oguchi, Y., Hachikubo, Y., Ishiwata, S. and Muto, E. (2010) Key residues on microtubule responsible for activation of kinesin ATPase. *EMBO J.*, **29**, 1167–1175.
18. Niwa, S., Takahashi, H. and Hirokawa, N. (2013) β-Tubulin mutations that cause severe neuropathies disrupt axonal transport. *EMBO J.*, **32**, 1352–1364.
19. Ti, S.C., Pamula, M.C., Howes, S.C., Duellberg, C., Cade, N.I., Kleiner, R.E., Forth, S., Surrey, T., Nogales, E. and Kapoor, T.M. (2016) Mutations in human tubulin proximal to the kinesin-binding site alter dynamic instability at microtubule plus- and minus-ends. *Dev. Cell*, **37**, 72–84.
20. Tischfield, M.A., Baris, H.N., Wu, C., Rudolph, G., Van Maldergem, L., He, W., Chan, W.M., Andrews, C., Demer, J.L., Robertson, R.L. *et al.* (2010) Human TUBB3 mutations perturb microtubule dynamics, kinesin interactions, and axon guidance. *Cell*, **140**, 74–87.
21. Hirokawa, N., Noda, Y., Tanaka, Y. and Niwa, S. (2009) Kinesin superfamily motor proteins and intracellular transport. *Nat. Rev. Mol. Cell Biol.*, **10**, 682–696.
22. Hirokawa, N., Niwa, S. and Tanaka, Y. (2010) Molecular motors in neurons: transport mechanisms and roles in brain function, development, and disease. *Neuron*, **68**, 610–638.
23. Cross, R.A. and McAinsh, A. (2014) Prime movers: the mechanochemistry of mitotic kinesins. *Nat. Rev. Mol. Cell Biol.*, **15**, 257–271.
24. Tubulinopathies Overview. Bahi-Buisson, N. and Cavallin, M. (2016) GeneReviews Seattle, WA: University of Washington, Seattle, 1993–2017, 2016. https://www.ncbi.nlm.nih.gov/books/NBK350554/.
25. Thomas, P. and Fenech, M. (2007) Chromosome 17 and 21 aneuploidy in buccal cells is increased with ageing and in Alzheimer's disease. *Mutagenesis*, **23**, 57–65.
26. Faggioli, F., Vijg, J. and Montagna, C. (2011) Chromosomal aneuploidy in the aging brain. *Mech. Aging Dev.*, **132**, 429–436.
27. Oromendia, A.B. and Amon, A. (2014) Aneuploidy: implications for protein homeostasis and disease. *Dis. Model. Mech.*, **7**, 15–20.
28. Siegel, J.J. and Amon, A. (2012) New insights into the troubles of aneuploidy. *Annu. Rev. Cell Dev. Biol.*, **28**, 189–214.
29. Sathasivam, K., Woodman, B., Mahal, A., Bertaux, F., Wanker, E.E., Shima, D.T. and Bates, G.P. (2001) Centrosome disorganization in fibroblast cultures derived from R6/2 Huntington's disease (HD) transgenic mice and HD patients. *Hum. Mol. Genet.*, **10**, 2425–2435.
30. Iourov, I.Y., Vorsanova, S.G., Liehr, T. and Yurov, Y.B. (2009) Aneuploidy in the normal, Alzheimer's disease and ataxia-telangiectasia brain: differential expression and pathological meaning. *Neurobiol. Dis.*, **34**, 212–220.
31. Mosch, B., Morawski, M., Mittag, A., Lenz, D., Tarnok, A. and Arendt, T.J. (2007) Aneuploidy and DNA replication in the normal human brain and Alzheimer's disease. *J. Neurosci.*, **27**, 6859–686
32. Yurov, Y.B., Vorsanova, S.G., Liehr, T., Kolotii, A.D. and Iourov, I.Y. (2014) X chromosome aneuploidy in the Alzheimer's disease brain. *Mol. Cytogenet.*, **7**, 20.
33. Arendt, T., Brückner, M.K., Mosch, B. and Lösche, A. (2010) Selective cell death of hyperploid neurons in Alzheimer's disease. *Am. J. Pathol.*, **177**, 15–20.
34. Okada, Y., Yamazaki, H., Sekine-Aizawa, Y. and Hirokawa, N. (1995) The neuron-specific kinesin superfamily protein KIF1A is a unique monomeric motor for anterograde axonal transport of synaptic vesicle precursors. *Cell*, **81**, 769–780.
35. Hotchkiss, L., Donkervoort, S., Leach, M.E., Mohassel, P., Bharucha-Goebel, D.X., Bradley, N., Nguyen, D., Hu, Y., Gurgel-Giannetti, J. and Bönnemann, C.G. (2016) Novel de novo mutations in KIF1A as a cause of hereditary spastic

paraplegia with progressive central nervous system involvement. *J. Child Neurol.*, **31**, 1114–1119.
36. Lee, J.R., Srour, M., Kim, D., Hamdan, F.F., Lim, S.H., Brunel-Guitton, C., Décarie, J.C., Rossignol, E., Mitchell, G.A., Schreiber, A. *et al.* (2015) De novo mutations in the motor domain of KIF1A cause cognitive impairment, spastic paraparesis, axonal neuropathy, and cerebellar atrophy. *Hum. Mutat.*, **36**, 69–78.
37. Esmaeeli, N.S., Madou, M.R., Sirajuddin, M., Fregeau, B., McKnight, D., Lexa, K., Strober, J., Spaeth, C., Hallinan, B.E., Smaoui, N. *et al.* (2015) De novo mutations in KIF1A cause progressive encephalopathy and brain atrophy. *Ann. Clin. Transl. Neurol.*, **2**, 623–635.
38. Tomaselli, P.J., Rossor, A.M., Horga, A., Laura, M., Blake, J.C., Houlden, H. and Reilly, M.M. (2017) A de novo dominant mutation in KIF1A associated with axonal neuropathy, spasticity and autism spectrum disorder. *J. Peripher. Nerv. Syst.* doi: 10.1111/jns.12235
39. Yonekawa, Y., Harada, A., Okada, Y., Funakoshi, T., Kanai, Y., Takei, Y., Terada, S., Noda, T. and Hirokawa, N. (1998) Defect in synaptic vesicle precursor transport and neuronal cell death in KIF1A motor protein-deficient mice. *J. Cell Biol.*, **141**, 431–441.
40. Borysov, S.I., Granic, A., Padmanabhan, J., Walczak, C.E. and Potter, H. (2011) Alzheimer Aβ disrupts the mitotic spindle and directly inhibits mitotic microtubule motors. *Cell Cycle*, **10**, 1397–1410.
41. Bougé, A.L. and Parmentier, M.L. (2016) Tau excess impairs mitosis and kinesin-5 function, leading to aneuploidy and cell death. *Dis. Model. Mech.*, **9**, 307–319.
42. Wordeman, L. (2010) How kinesin motor proteins drive mitotic spindle function: lessons from molecular assays. *Semin. Cell Dev. Biol.*, **21**, 260–268.
43. Goshima, G. and Vale, R.D. (2003) The roles of microtubule-based motor proteins in mitosis comprehensive RNAi analysis in the Drosophila S2 cell line. *J. Cell Biol.*, **162**, 1003–1016.
44. Blangy, A., Lane, H.A., D'Herin, P., Harper, M., Kress, S.M. and Nigg, E.A. (1995) Phosphorylation by p34cdc2 regulates spindle association of human Eg5, a kinesin-related motor essential for bipolar spindle formation in vivo. *Cell*, **63**, 1159–1169.
45. Heck, M.M., Pereira, A., Pesavento, P., Yannoni, Y., Spradling, A.C. and Goldstein, L.S.B. (1993) The kinesin-like protein KLP61F is essential for mitosis in Drosophila. *J. Cell Biol.*, **123**, 665–679.
46. Hoyt, M.A., He, L., Loo, K.K. and Saunders, W.S. (1992) Two *Saccharomyces cerevisiae* kinesin-rrelated gene products required for mitotic spindle assembly. *J. Cell Biol.*, **118**, 109–120.
47. Roof, D.M., Meluh, P.B. and Rose, M.D. (1992) Kinesin-related proteins required for the assembly of the mitotic spindle. *J. Cell Biol.*, **118**, 95–108.
48. Sawin, K.E., LeGuellec, K., Philippe, M. and Mitchison, T.J. (1992) Mitotic spindle organization by a plus-end directed microtubule motor. *Nature*, **359**, 540–543.
49. Saunders, W.S. and Hoyt, M.A. (1992) Kinesin-related proteins required for the structural integrity of the mitotic spindle. *Cell*, **70**, 451–458.
50. Zhao, C., Takita, J., Tanaka, Y., Setou, M., Nakagawa, T., Takeda, S., Yang, H.W., Terada, S., Nakata, T., Takei, Y. *et al.* (2001) Charcot-Marie-Tooth disease type 2A caused by mutation in a microtubule motor KIF1Bbeta. *Cell*, **105**, 587–597.
51. Dor, T., Cinnamon, Y., Raymond, L., Shaag, A., Bouslam, N., Bouhouche, A., Gaussen, M., Meyer, V., Durr, A., Brice, A. *et al.* (2014) KIF1C mutations in two families with hereditary spastic paraparesis and cerebellar dysfunction. *J. Med. Genet.*, **51**, 137–142.
52. Caballero Oteyza, A., Battalo lu, E., Ocek, L., Lindig, T., Reichbauer, J., Rebelo, A.P., Gonzalez, M.A., Zorlu, Y., Ozes, B., Timmann, D. *et al.* (2014) Motor protein mutations cause a new form of hereditary spastic paraplegia. *Neurology*, **82**, 2007–2016.
53. Niceta, M., Stellacci, E., Gripp, K.W. and Tartaglia, M. (2015) Mutations impairing GSK3-mediated MAF phosphorylation cause cataract, deafness, intellectual disability, seizures, and a down syndrome-like facies. *Am. J. Hum. Genet.*, **96**, 816–825.
54. Flex, E., Niceta, M., Cecchetti, S., Thiffault, I., Au, M.G., Capuano, A., Piermarini, E., Ivanova, A.A., Francis, J.W., Chillemi, G. *et al.* (2016) Biallelic mutations in TBCD, encoding the tubulin folding cofactor D, perturb microtubule dynamics and cause early-onset encephalopathy. *Am. J. Hum. Genet.*, **99**, 962–973.
55. Sferra, A., Baillat, G., Rizza, T., Barresi, S., Flex, E., Tasca, G., D'Amico, A., Bellacchio, E., Ciolfi, A., Caputo, V. *et al.* (2016) TBCE mutations cause early-onset progressive encephalopathy with distal spinal muscular atrophy. *Am. J. Hum. Genet.*, **99**, 974–983.
56. Lek, M., Karczewski, K.J., Minikel, E.V., Samocha, K.E., Banks, E., Fennell, T., O'Donnell-Luria, A.H., Ware, J.S., Hill, A.J., Cummings, B.B. *et al.* (2016) Exome Aggregation Consortium. Analysis of protein-coding genetic variation in 60, 706 humans. *Nature*, **536**, 285–291.
57. Cingolani, P., Platts, A., Wang le, L., Coon, M., Nguyen, T., Wang, L., Land, S.J., Lu, X. and Ruden, D.M. (2012) A program for annotating and predicting the effects of single nucleotide polymorphisms, SnpEff: SNPs in the genome of Drosophila melanogaster strain w1118. *Fly*, **6**, 80–92.
58. Liu, X., Wu, C., Li, C. and Boerwinkle, E. (2016) dbNSFP v3.0: a one-stop database of functional predictions and annotations for human nonsynonymous and splice-site SNVs. *Hum. Mutat.*, **37**, 235–241.
59. Kircher, M., Witten, D.M., Jain, P., O'Roak, B.J., Cooper, G.M. and Shendure, J. (2014) A general framework for estimating the relative pathogenicity of human genetic variants. *Nat. Genet.*, **46**, 310–315.
60. Nagata, K., Randall, A. and Baldi, P. (2012) SIDEpro: a novel machine learning approach for the fast and accurate prediction of side-chain conformations. *Proteins*, **80**, 142–153.